CHAPTER-4

Evolution of Relaxor Type High-k Dielectric in Bulk Pristine Cu^{2+} and Li^{+} co-substituted Wurtzite ZnO

4.1 INTRODUCTION

The dielectric constant of material ultimately decides the level of miniaturization in electronic devices based on capacitive components [1-3]. In the past decades, Due to its low cost [4-7], non-toxicity [8,9], and bio-compatibility [10], ZnO has attracted a great deal of attention for a wide range of applications including dielectrics as well as photocatalyst, sensors, and in dilute magnetism. Although the dielectric properties of ZnO nanostructures, films, and ceramics have been investigated by many researchers, further improvements are still required before they become usable for commercial applications [2,3]. Moreover, it is quite abundant and can be easily fabricated for thin films for various applications [11,12]. In addition, ZnO is also employed in a wide range of applications such as sensors [13], light-emitting devices [14-16], solar cell electrodes [17], optical waveguide devices [18-20], optoelectronic devices[21 -25]. The direct band gap of ZnO is about 3.37 eV [26,27] with a high binding energy of about 60 meV and an intrinsic n-type conductivity[28]. The doping of ZnO thin film is carried out to enhance the microstructural, optical, and electrical performances.[29,30] Indeed, the choice of the dopants depends on the required applications. It is well established that the physical characteristics of nanomaterials are affected by the size and morphology of nanoparticles. The increase in the surface/volume ratio due to the decrease in the size of the crystallites allows surface defects to play an important role in all surface phenomena such as gas adsorption [31-33], wettability [34,35], photocatalytic activities [36]. Moreover, it is well understood that a rise in the size of crystallite can affect the optical properties of oxide thin films (gap optics, transparency)[37] as well as their electrical conductivities [38].

4.2 Material Synthesis and Characterizations:

In this chapter, $Zn_{0.92}Cu_{0.05}Li_{0.03}O_{1-\delta}$ and $Zn_{0.9}Cu_{0.05}Li_{0.05}O_{1-\delta}$ ceramic samples were prepared by the conventional sol-gel method. In these samples, we doped Cu and Li in ZnO to get the combined effects of the dopant on the dielectric properties of the material. We have taken the stoichiometric amount of ZnO, LiCl, and $CuCl_2$ for the synthesis. After gel formation, we put the gel in the oven at 200 °C to dry. After that, we ground it and put it in the furnace at 950 °C for 12 hrs. The phase formation study was carried out through a Rigaku Miniflex desktop X-ray diffractometer (XRD) with Cu-Kα radiation (λ = 1.54 Å) in the 2θ range of 20−80° with a step size of 0.02°. The structures were refined by the Rietveld refinement method using FULLPROF suite software package 31 and wurtzite ZnO (space group: P63mc) as the model structure. The microstructures of the sintered samples were investigated using scanning electron microscopy (SEM, EVO-scanning electron microscope MA15/18). The average grain size was calculated using the linear intercept method. The composition of the compounds was examined by energy dispersive X-ray (EDX) spectroscopy with a probe attached to the SEM instrument. X-ray photoelectron spectroscopy (XPS) studies were carried out to examine the electronic structure of the materials. XPS of the samples were collected using a Thermo Scientific Multilab 2000 instrument by employing an Al-Kα radiation source operated at 150 kW. Binding energies were corrected and reported here concerning C(1s) at 284.5 eV, and they are accurate within ±0.1 eV. Fourier transform infrared (FT-IR) spectra were measured using the KBr method on a Fourier transform infrared spectrometer at RT in the range of 4000–400 cm^{-1} with a resolution of 1 cm^{-1}.

All samples were examined by using a Novocontrol Alpha-A frequency analyzer for dielectric measurements. The dielectric, modulus, and loss measurements as well as impedance measurements were carried out for all the samples. The measurements were done in the frequency range 1 Hz to 10^6 Hz in the temperature range of room temperature (25 ^{o}C) to 650°C. For the study, we did silver plating on the pellet and then put it in the Novo control Alpha-A frequency analyzer, and then we did heating by the furnace from room temperature to 650°C and we took readings at the various points.

For the ferroelectric studies, polishing of the pellets was carried out by fine grain size emery paper followed by heat treatment at 650 ^{o}C to remove residual stresses from the pellet. After that electrode was done on both sides of the pellet by silver paste. Further pellet was heated at 400^{o}C for 1 hour to dry the electrodes fabricated on the pellet. Ferroelectric measurement was carried out at room temperature from 100 Hz to 500 Hz frequency range using RADIANT precision premier II. For magnetic studies of our sample $Zn_{0.9}Cu_{0.05}Li_{0.05}O_{1-\delta}$, the fine ground powder was subjected to a Magnetic property measurement system (MPMS) by Squid-based magnetometer (MPMS-3, Quantum Design Inc.)

4.3 XRD Analysis

The structural parameters and phase purity were examined using powder X-ray diffraction patterns. XRD patterns of $Zn_{0.92}Cu_{0.05}Li_{0.03}O_{1-\delta}$ and $Zn_{0.9}Cu_{0.05}Li_{0.05}O_{1-\delta}$ are shown in Fig. 4.1(a). Sharp and intense diffraction peaks of all the samples confirm the high crystallinity of the samples. It also reveals phase formation (s.g. P63mc) in hexagonal wurtzite ZnO structure for full doping range. At higher Cu and Li dopings, impurities were identified. That is why we restricted the study to 5% Cu and Li (total 10%) doped samples only. The structures were refined by the Rietveld refinement method using FULLPROF suite software package 31 and wurtzite ZnO (space group: P63mc) as the model structure. The refined Rietveld is given in Figure 4.1 (b and c).

Table 4.1. Structural Parameters of $Zn_{0.92}Cu_{0.05}Li_{0.03}O_{1-\delta}$ and $Zn_{0.9}Cu_{0.05}Li_{0.05}O_{1-\delta}$

Compound	Lattice Parameters (Å)		χ^2	R_f	R_{Bragg}	R_{wp}
	a=b	C				
$Zn_{0.92}Cu_{0.05}Li_{0.03}O$	3.25197	5.20552	1.36	6.73	7.20	17.9
$Zn_{0.9}Cu_{0.05}Li_{0.05}O$	3.25206	5.20323	1.78	7.21	6.18	16.7

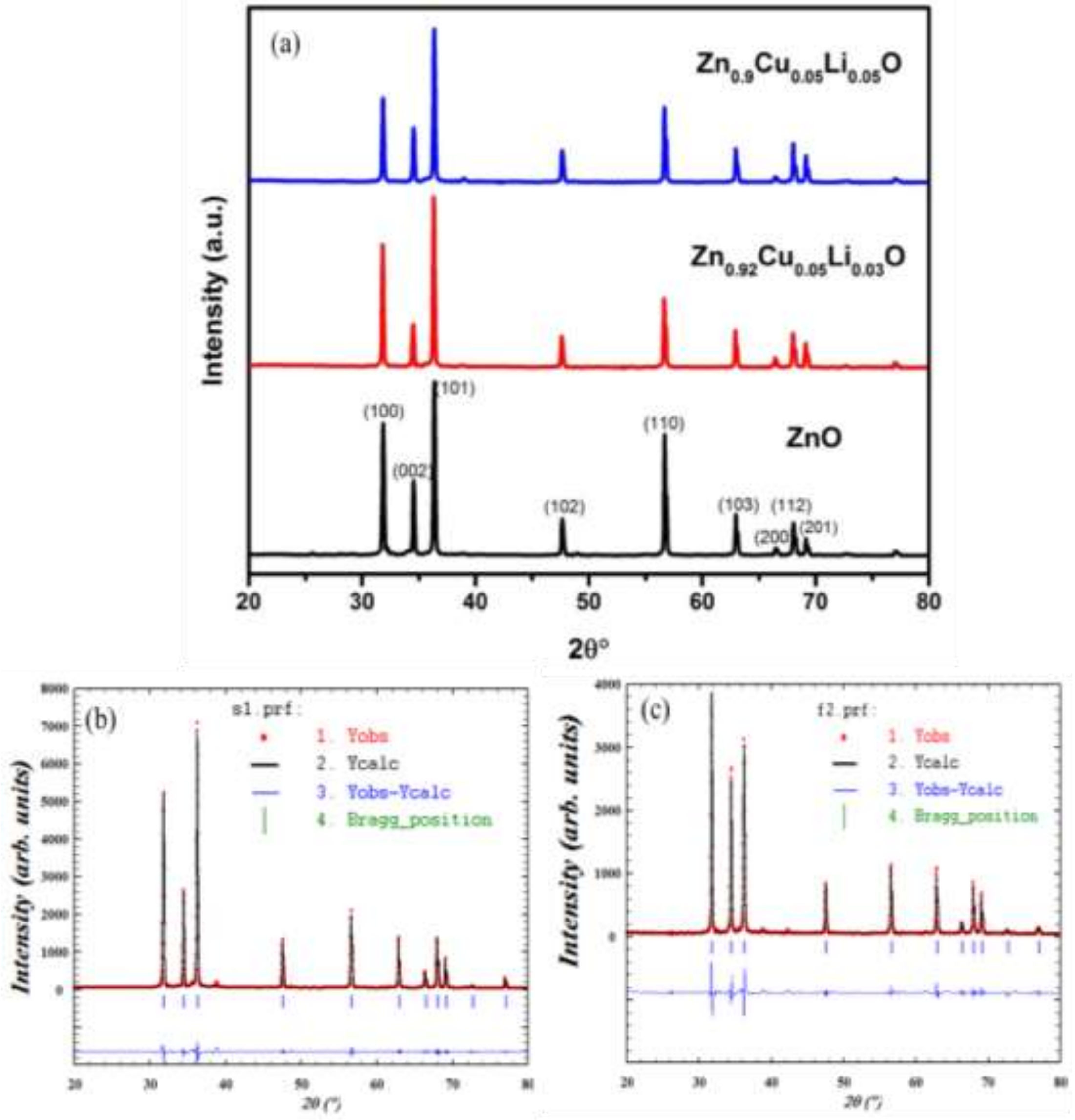

Figure 4.1 (a) Powder XRD pattern of ZnO, $Zn_{0.92}Cu_{0.05}Li_{0.03}O_{1-\delta}$, and $Zn_{0.9}Cu_{0.05}Li_{0.05}O_{1-\delta}$. Rietveld refined powder XRD pattern of (b) $Zn_{0.92}Cu_{0.05}Li_{0.03}O_{1-\delta}$ and (c) $Zn_{0.9}Cu_{0.05}Li_{0.05}O_{1-\delta}$

4.4 SEM and EDAX Study

The SEM study of broken pellets of $Zn_{0.92}Cu_{0.05}Li_{0.03}O_{1-\delta}$ and $Zn_{0.9}Cu_{0.05}Li_{0.05}O_{1-\delta}$ reveals that the grains are interconnected well with each other and are of micrometer sizes in the range of 2–50 µm (Figure 4.2(a) and 4.3(a)). The EDX image shown in Fig. 4.2(b) and 4.3(b) also confirms the composition and apparent homogeneity of the materials; however, Li peaks do not appear in the EDX image due to spectroscopic limitations in the EDX study.

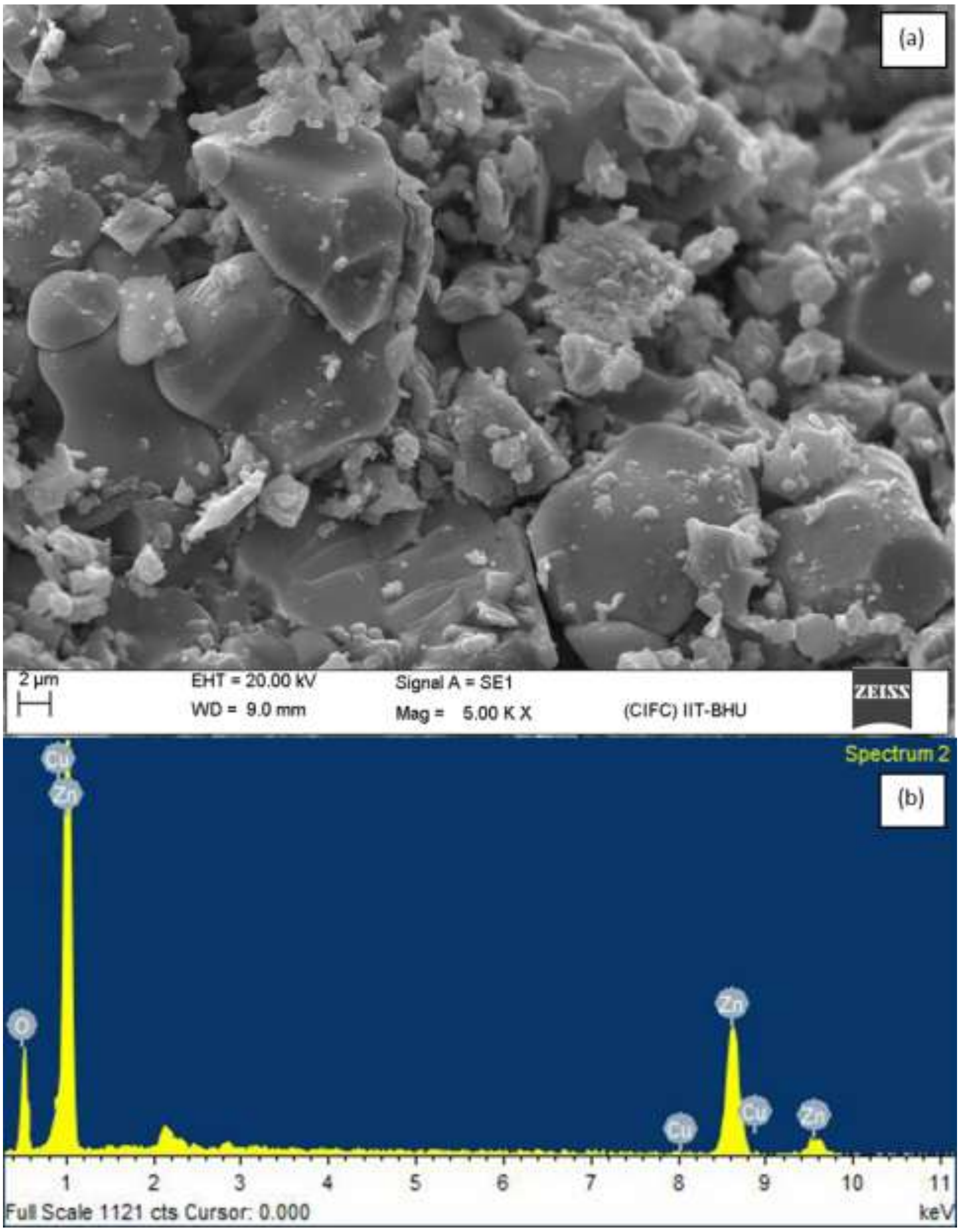

Figure 4.2 (a) SEM image and (b) EDAX image of $Zn_{0.92}Cu_{0.05}Li_{0.03}O_{1-\delta}$.

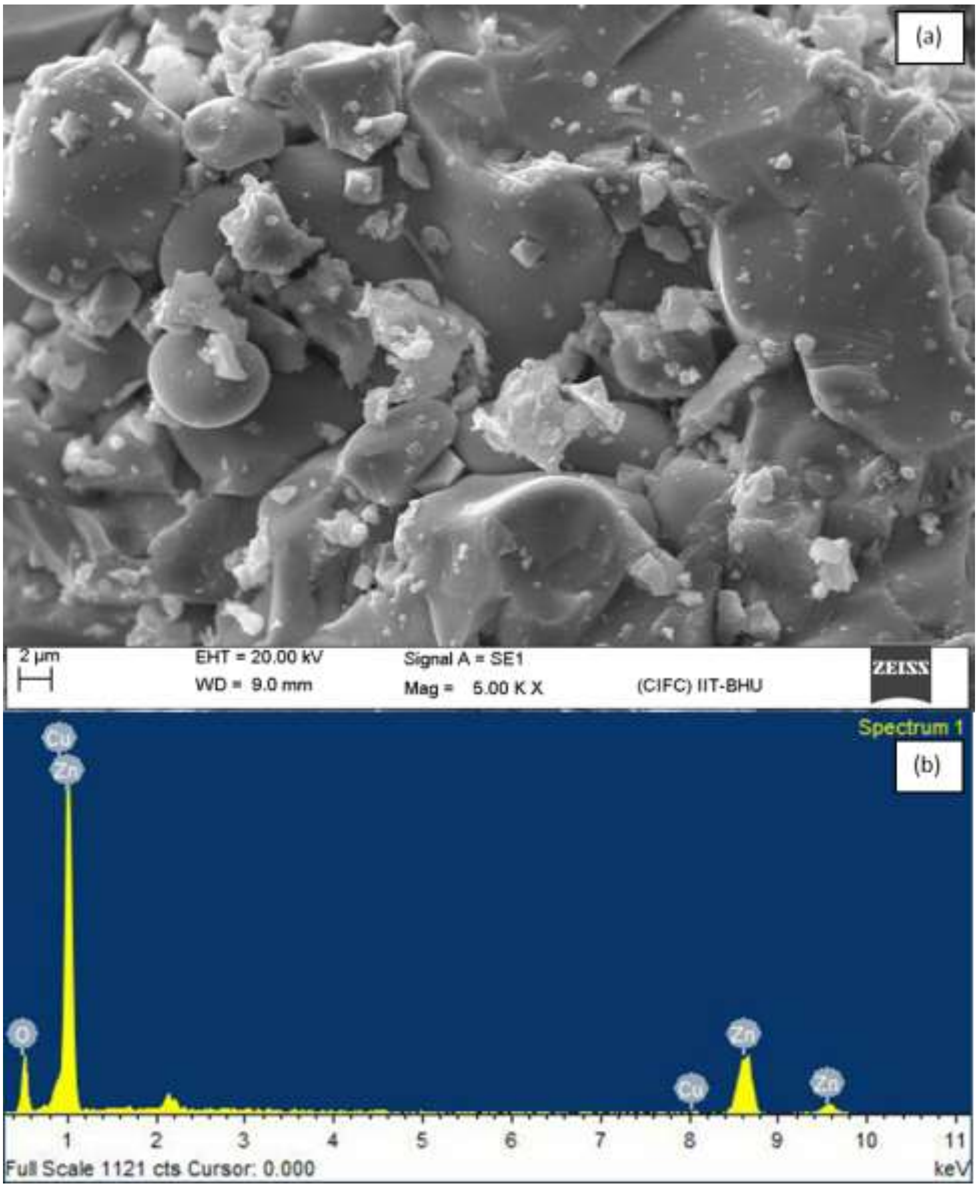

Figure. 4.3. (a). SEM image and (b). EDAX image of $Zn_{0.9}Cu_{0.05}Li_{0.05}O_{1-\delta}$.

4.5 XPS Study

Electronic structure materials were investigated by the XPS study. Figure 4.4(a) shows the survey spectra of the XPS study of the $Zn_{0.9}Cu_{0.05}Li_{0.05}O_{1-\delta}$ pellet. The deconvoluted Li(1s) and Cu(2p) spectra are shown in Figure 4.4 (b) and (c). Core level 1s peak lithium was observed at 55.4 eV confirming the presence of Li in the sample. The 2p3/2 peaks marked at 933.5 with strong satellite at 942.1 eV and 2p1/2 at 952.6 eV with corresponding satellite peak at 961.8 eV, respectively, confirm the presence of Cu^{2+} in the sample. The 2p3/2 and 2p1/2 peaks at 1021.2 eV and 1044.8 eV respectively in Figure 4.4(d) were assigned to Zn^{2+} ions.

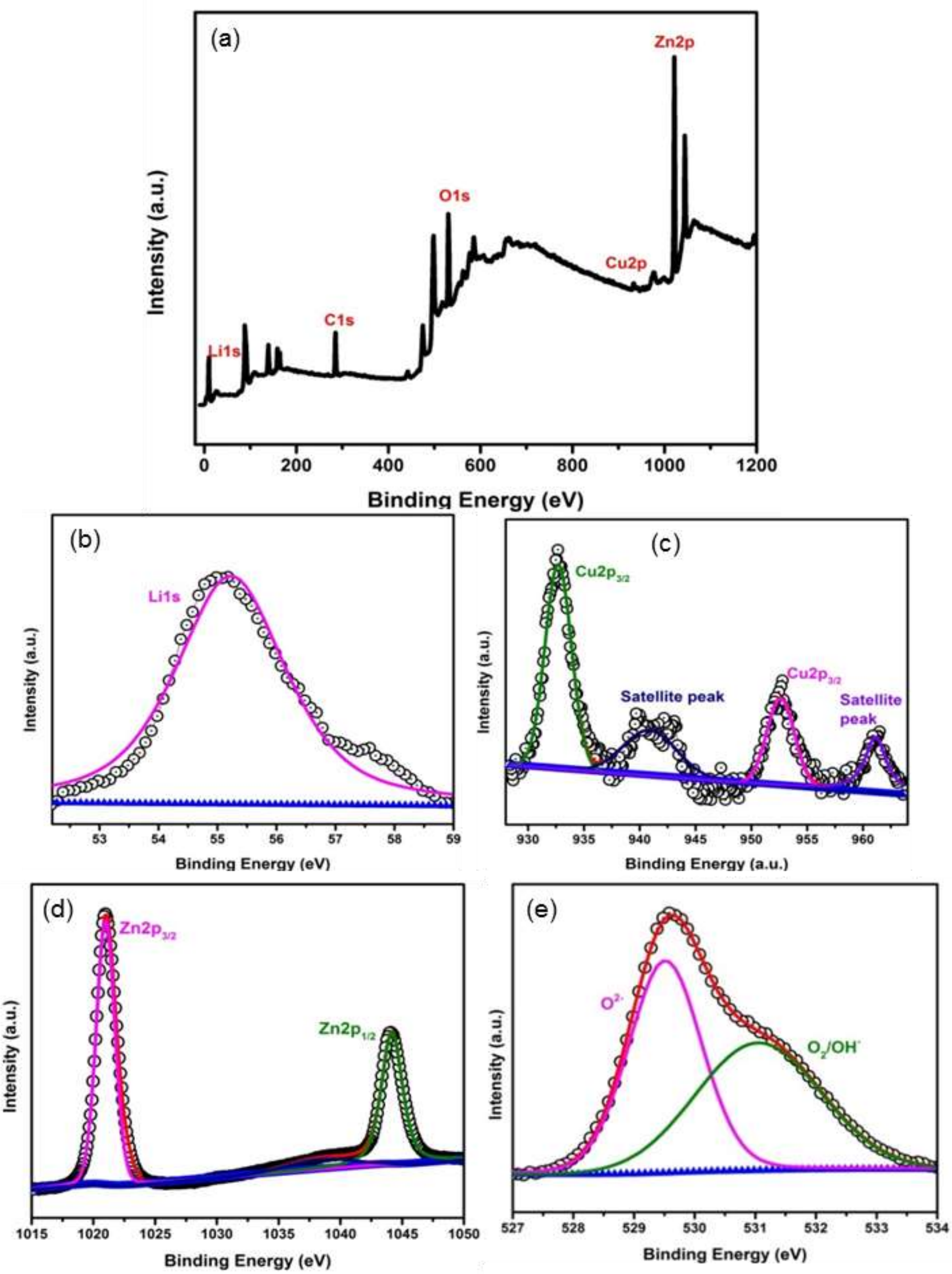

Figure: 4.4. XPS of $Zn_{0.9}Cu_{0.05}Li_{0.05}O_{1-\delta}$ (a) Full survey, (b) Core level of Li(1s), (c) Core level of Cu(2p), (d) Core level of Zn(2p), (e) Core level of O(1s).

Figure 4.4(e) shows the O(1s) core level spectra. The O(1s) spectra are deconvoluted into four characteristic peaks: (1) the lattice oxygen species peak at ≈528.6 eV for O2−, (2) the highly oxidative oxygen species peak at ≈529.96 eV due to oxygen vacancy or hydroxide/absorbed water molecule on lattice oxygen vacancies.

4.6 FTIR Study

Figure 4.5 shows the FTIR spectra of $Zn_{0.9}Cu_{0.05}Li_{0.05}O_{1-\delta}$. The spectrum of $Zn_{0.9}Cu_{0.05}Li_{0.05}O_{1-\delta}$ shows a strong band at 505 cm^{-1}, which corresponds to Zn–O bonding [39]. With the addition of Li and Cu, this mode gets broadened slightly due to the incorporation of Li and Cu into ZnO. The presence of organic groups on the surface of the material is known from the modes at the higher wavenumber region of the FTIR spectrum. The broad band at around 3470 cm^{-1} is due to the presence of O–H groups.[40] The band at around 1560 cm^{-1} shows the sharp peaks of the $Zn_{0.9}Cu_{0.05}Li_{0.05}O_{1-\delta}$ sample as compared to the pure ZnO sample. This may be due to the incorporation of Li and Cu in ZnO.[41]

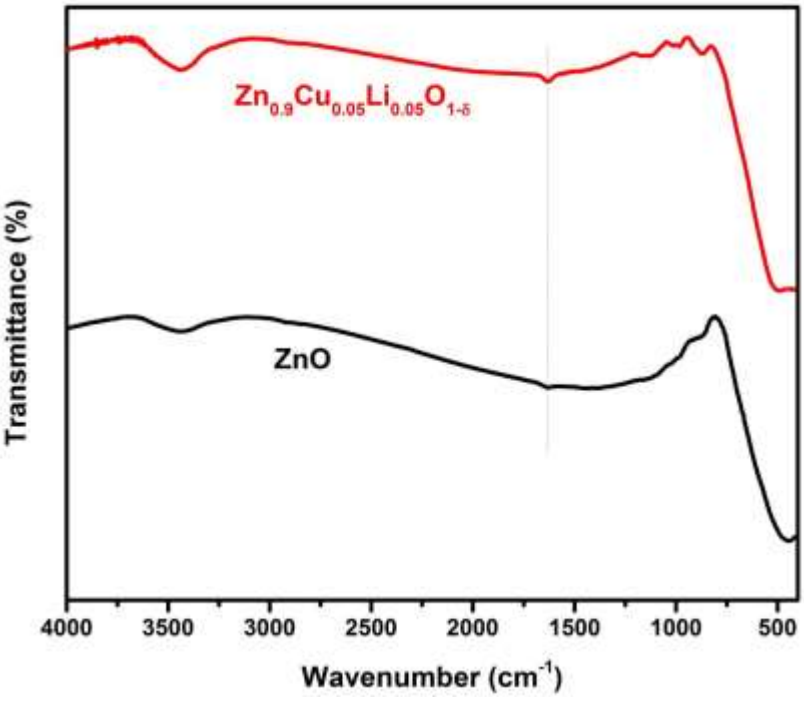

Figure: 4.5. FTIR spectra of $Zn_{0.9}Cu_{0.05}Li_{0.05}O_{1-\delta}$ at RT.

4.7 Impedance Study

Figures 4.6(a) and 4.7(a) show the plots of the real part of the dielectric constant (ε_r') at 100 Hz to 100kHz frequency range for the $Zn_{0.92}Cu_{0.05}Li_{0.03}O$ and $Zn_{0.9}Cu_{0.05}Li_{0.05}O$ pellets in the temperature range of RT to 650°C. In general, the ε_r' values were increasing in the range of RT to 650°C with maxima (T_m) appearing around 600°C. The dielectric constant (ε_r') for $Zn_{0.92}Cu_{0.05}Li_{0.03}O$ and $Zn_{0.9}Cu_{0.05}Li_{0.05}O$ is found to be 18000 and 20000 respectively at 1000 Hz frequency at 600°C. We believe that the alignment to the net dipole moment on oxygen vacant polyhedral in Cu^{2+} and Li^{+} doped ZnO lattice results very high dielectric constant at lower frequencies. At higher frequencies, the effect of oxygen vacancies in the lattice gets minimized and also we found that the T_m is increasing with increasing frequencies suggesting the relaxor nature of the dielectricity in the materials. The variation in dielectric loss ($\tan \delta = \varepsilon_r''/\varepsilon_r'$) with temperature, at the selected frequency, is shown in Figures 4.6(b) and 4.7(b). Considering the high dielectric constant of the materials, the observed dielectric loss is quite less for $Zn_{0.92}Cu_{0.05}Li_{0.03}O_{1-\delta}$ and $Zn_{0.9}Cu_{0.05}Li_{0.05}O_{1-\delta}$ samples. It was found that the dielectric constant was increasing continuously up to 600 °C and dielectric loss was first increasing up to 300 °C and then decreasing in the temperature range from 300 °C to 650 °C at all frequencies. Again we found that T_m is increasing with increasing frequencies suggesting the relaxor nature of dielectricty in the sample. Both dielectric constant and dielectric loss were decreasing with increasing frequencies. The increase in dielectric constant (ε_r') with increasing temperatures at different frequencies for $Zn_{0.92}Cu_{0.05}Li_{0.03}O_{1-\delta}$ and $Zn_{0.9}Cu_{0.05}Li_{0.05}O_{1-\delta}$ is likely due to the localized nature of hopping charge carriers in addition to interfacial polarization due to space charge. These extrinsic contributions to ε_r' are expected to contribute significantly only at higher frequencies. Further from

Fig. 4.8(a, b) and 4.9(a, b) of $Zn_{0.92}Cu_{0.05}Li_{0.03}O_{1-\delta}$ and $Zn_{0.9}Cu_{0.05}Li_{0.05}O_{1-\delta}$, confirms that at lower frequencies high relative dielectric permittivity was found. The dispersion of dielectric properties is obvious. The formation of the grain boundary barrier layer was also confirmed by the non-ohmic I–V behavior and the quick drop of apparent dielectric constant with increasing frequency of the samples. The large frequency dispersion never reached a low-frequency plateau. Inhomogeneities in grains and/or the presence of potential barriers between the grains are considered to be the reason for similar dielectric properties in many materials.

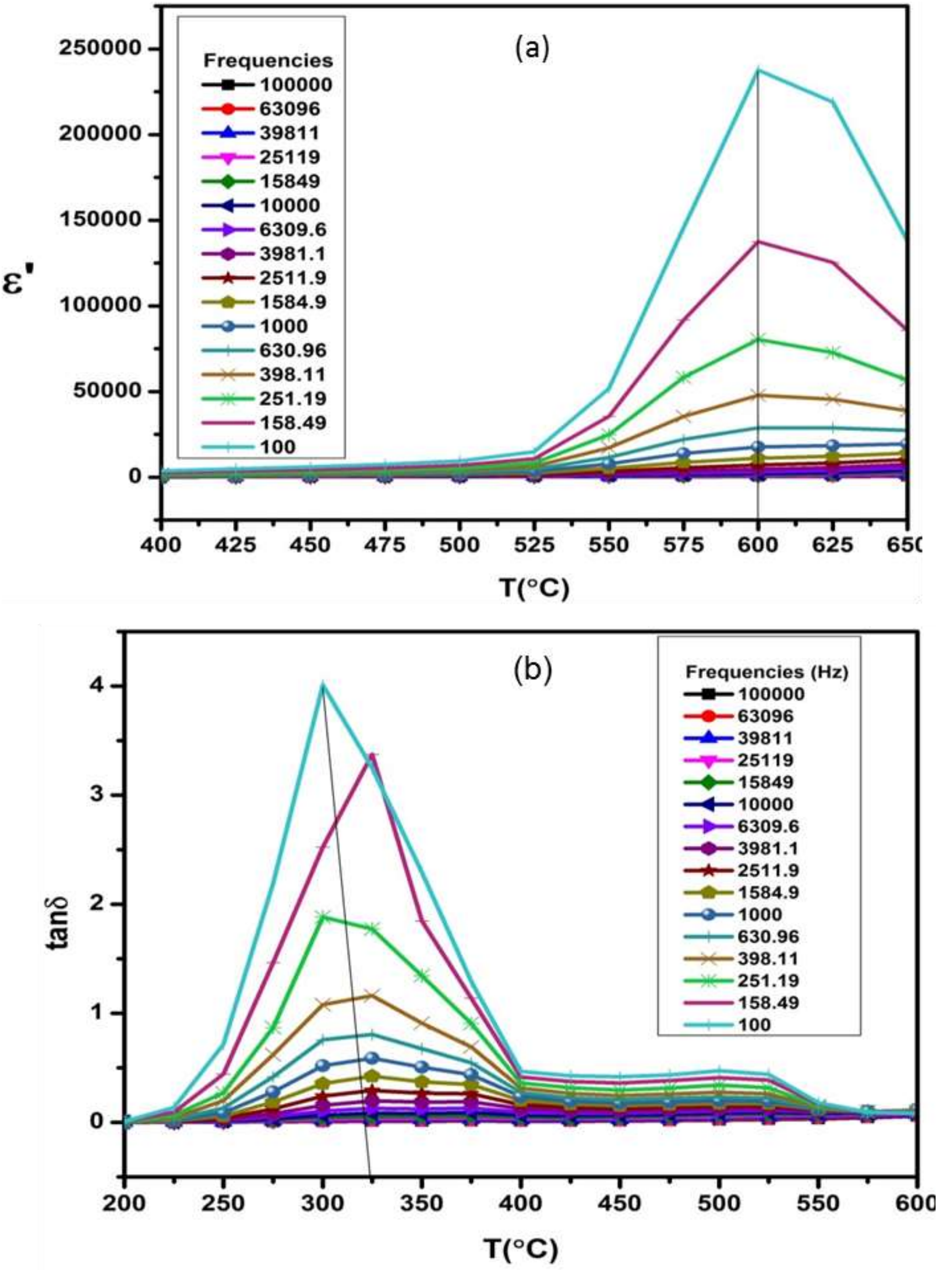

Figure. 4.6. (a). Dielectric constant and (b). Dilelectric loss of $Zn_{0.92}Cu_{0.05}Li_{0.03}O_{1-\delta}$

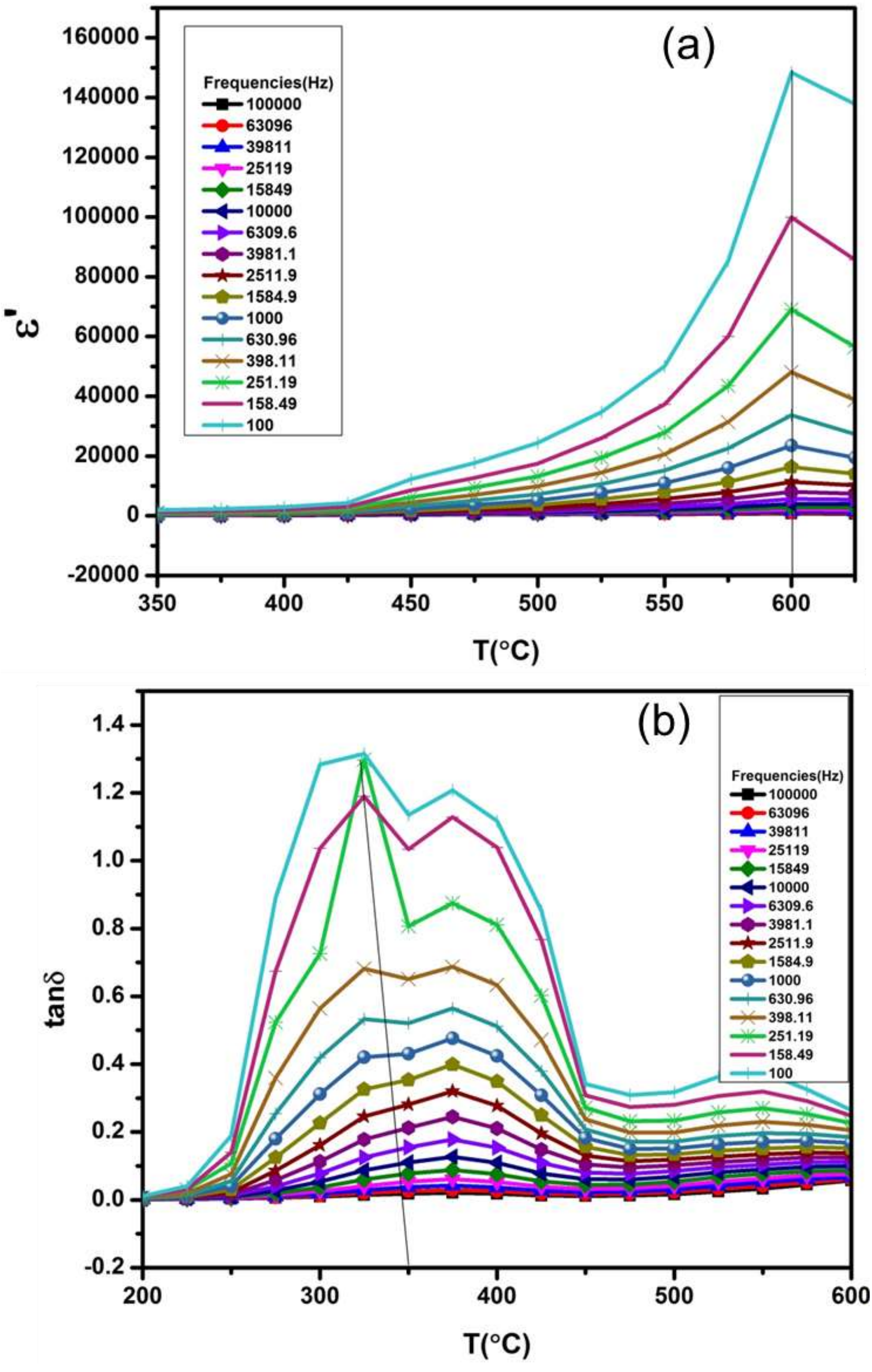

Figure. 4.7 (a). Dielectric constant and (b). Dilelectric loss of $Zn_{0.9}Cu_{0.05}Li_{0.05}O_{1-\delta}$.

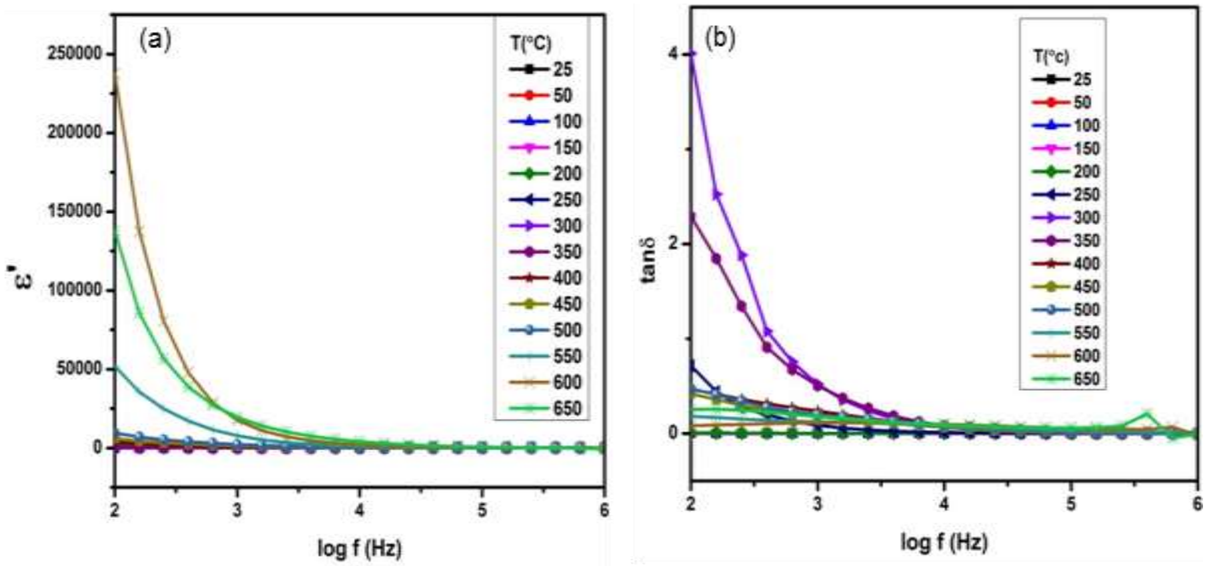

Figure. 4.8 (a). ε_r vs. log frequency plot, (b). tanδ vs. log frequency plot of

$Zn_{0.92}Cu_{0.05}Li_{0.03}O_{1-\delta}$

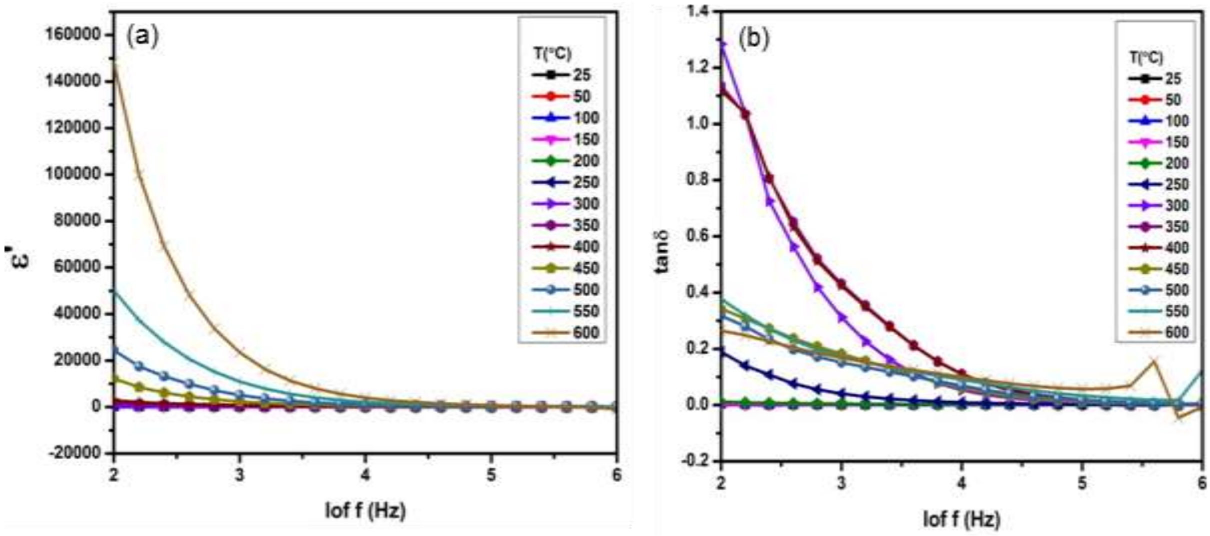

Figure. 4.9 (a) ε_r vs. log frequency plot, (b) tanδ vs. log frequency plot of

$Zn_{0.9}Cu_{0.05}Li_{0.05}O_{1-\delta}$.

Overall, doping of Cu^{2+} and Li^{+} in the ZnO lattice has proven to be an important strategy to improve the dielectric constant of the ZnO base materials. Further co-doping Cu^{2+} and Li^{+} in resulted relaxor type dielectricity in the materials.

4.8 MPMS Study

To understand the electronic structure of the $Zn_{0.9}Cu_{0.05}Li_{0.05}O_{1-\delta}$ sample, the magnetic response of the $Zn_{0.9}Cu_{0.05}Li_{0.05}O_{1-\delta}$ was also studied using a Magnetic property measurement system (MPMS) by Squid based magnetometer (MPMS-3, Quantum Design Inc.). Figure 4.10 shows a typical magnetization vs. magnetic field (M-H) curve obtained from a $Zn_{0.9}Cu_{0.05}Li_{0.05}O_{1-\delta}$ sample at 5K and 300K. From the curve, it can be inferred that $Zn_{0.9}Cu_{0.05}Li_{0.05}O_{1-\delta}$ exhibiting the ferromagnetic behavior with a noticeable coercitivity and saturation magnetization at 300K were 84 Oe and 6.63 memu/g respectively, and 114 Oe and 7.43 memu/g at 5K respectively.

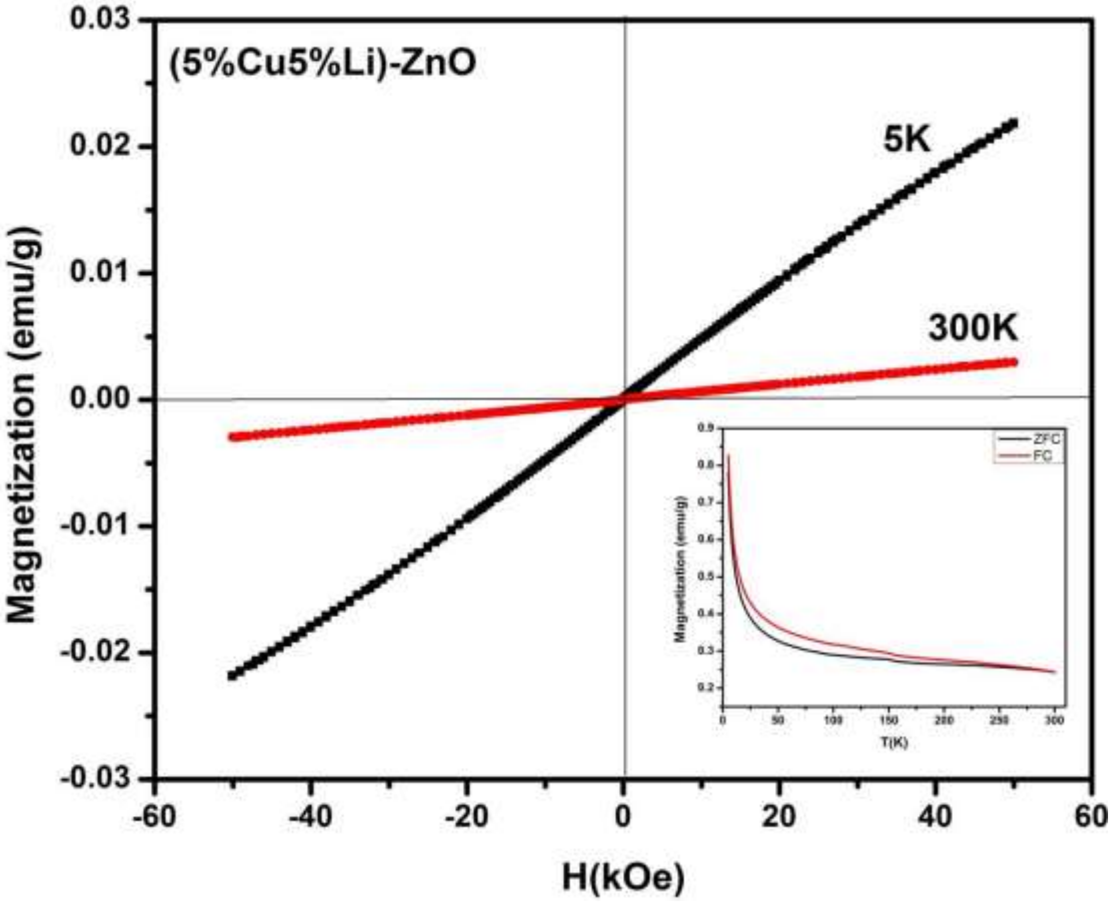

Figure. 4.10. M-H curve of $Zn_{0.9}Cu_{0.05}Li_{0.05}O_{1-\delta}$ and inset shows M-T curve of $Zn_{0.9}Cu_{0.05}Li_{0.05}O_{1-\delta}$.

4.9 P-E Loop Study

Bulk $Zn_{0.9}Cu_{0.05}Li_{0.05}O_{1-\delta}$ also exhibits ferroelectricity at room temperature with remnant polarization Pr and Vc equal to $4.20*10^{-02}$ μC/cm^2 and $4.1*10^{+03}$ V/cm at (30KV, 500 Hz) respectively in figure 4.11. However, the other materials of Cu, Li, and Zn systems from the thin film have relatively higher values for ferroelectricity, the values of the $Zn_{0.9}Cu_{0.05}Li_{0.05}O_{1-\delta}$ were investigated. As the frequency increases, the maximum polarization decreases. The shape of the P–E loops and the remanent polarization were found to exhibit little frequency dependence.

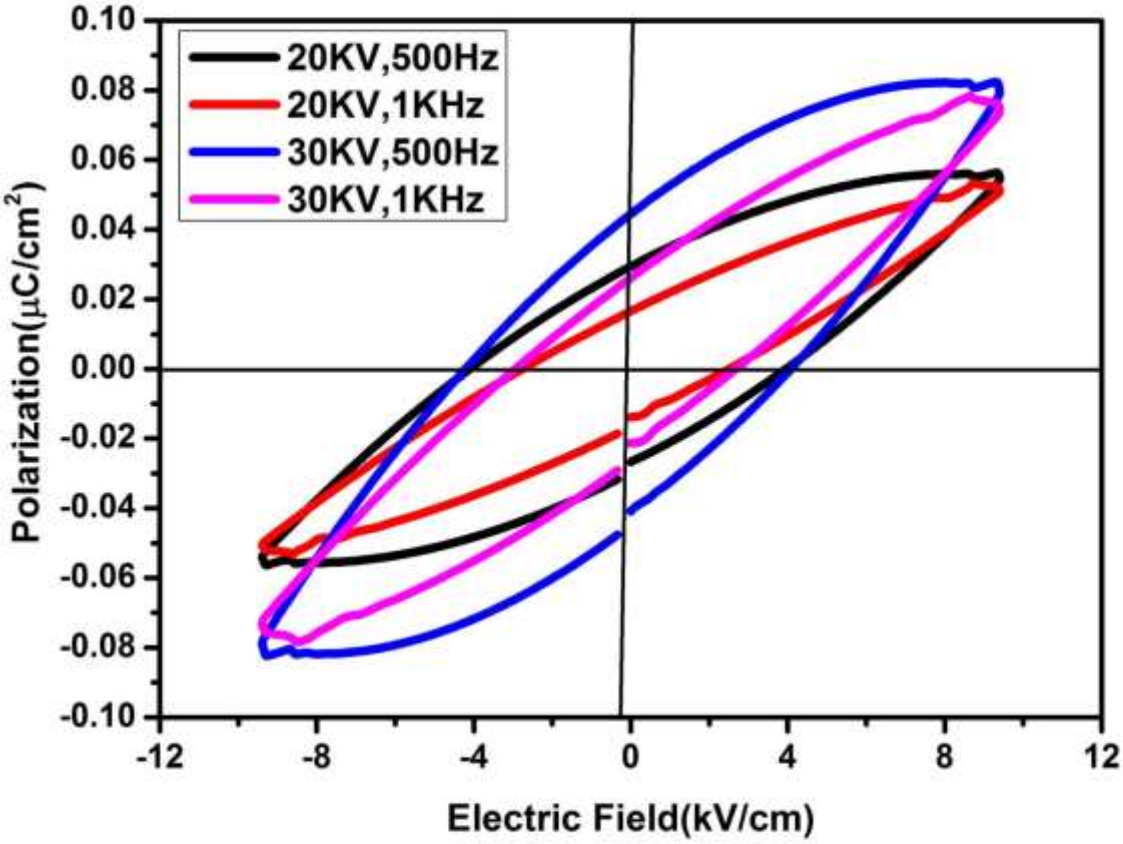

Fig. 4.11. Polarization versus electrical field (P–E) hysteresis loops of $Zn_{0.9}Cu_{0.05}Li_{0.05}O_{1-\delta}$.

4.10 Conclusion

Synthesis of single-phase Cu/Li co-doped ZnO was demonstrated in the study. In this work, $Zn_{0.92}Cu_{0.05}Li_{0.03}O_{1-\delta}$ and $Zn_{0.9}Cu_{0.05}Li_{0.05}O_{1-\delta}$ ceramics samples were prepared by the modified sol-gel method. However, we are not able to achieve more than 10% doping of Cu and Li in ZnO. The formation of single-phase wurtzite samples was confirmed by X-ray diffraction analysis. The microstructure of the material was analyzed by scanning electron microscopy which shows the polycrystalline nature of the samples and the composition of the sample were analyzed by an EDX probe attached SEM instrument. The bulk as well as surface composition of the sample were confirmed by ICP_MS and XPS study. The electronic structure and oxidation state of an element present in the sample were confirmed by the XPS study. The complex impedance spectroscopic study of Cu/Li co-doped ZnO confirms the high dielectric constant and low dielectric loss at high temperatures and high frequency compared to ZnO. The Cu/Li doping depresses the concentration of intrinsic donors and impedes the conduction mechanism. The effect of relative iconicity in the M-O (M = Zn, Cu, and Li) bond will result in effective net polarization in the lattice. Also with an increase of frequency, the dielectric constant and dielectric loss were found to decrease. This behavior was attributed to different hopping mechanisms and defects formed during synthesis. T_m was found to increase with increasing frequencies suggesting the relaxor nature of dielectricty in the sample and confirming that the co-doing Cu^{2+} and Li^{+} in ZnO resulted in relaxor-type dielectricty in the materials. The material $Zn_{0.9}Cu_{0.05}Li_{0.05}O_{1-\delta}$ also exhibits ferroelectricity and dilute magnetic property at room temperature.

REFERENCES

[1] C.C. Homes, T. Vogt, S.M. Shapiro, S. Wakimoto, A.P. Ramirez, Optical response of high-dielectric-constant perovskite-related oxide Science, 293 (2001), 673-676

[2] R. Tripathi, A. Kumar, C. Bharti, T.P. Sinha, Dielectric relaxation of ZnO nanostructure synthesized by soft chemical method, Curr. Appl. Phys., 10 (2010), 676-681

[3] M.K. Gupta, B. Kumar, Enhanced ferroelectric, dielectric and optical behavior in Li-doped ZnO nanorods, J. Alloys Compd., 509 (2011), L208-L212

[4] G. Corro, S. Cebada, F. Bañuelos, J.L.G. Fierro, U. Pal, E. Guilleminot, Low-cost Cu/ZnO as low temperature (150 °C) catalyst for diesel particulate matter oxidation, Top. Catal. 59, (2016) 1090–1094

[5] S.M. Mohammad, Z. Hassan, N.M. Ahmed, N.H. Al-Hardan, M. Bououdina Fabrication of low-cost UV photodetector using ZnO nanorods grown onto nylon substrate, J. Mater. Sci. Mater. Electron 26, (2015) 1322–1331

[6] K.H. Choi, M. Mustafa, K. Rahman, B.K. Jeong, Y.H. Doh, Cost-effective fabrication of memristive devices with ZnO thin film using printed electronics technologies, Appl. Phys. A 106, (2012) 165–170

[7] J.V. Gohel, A.K. Jana, M. Singh, Highly enhanced photocurrent of novel quantum-dot-co-sensitized PbS–Hg/CdS/Cu: ZnO thin films for photoelectrochemical applications, Appl. Phys. A 123, (2017) 506

[8] C. Karunakaran, A. Vijayabalan, P. Vinayagamoorthy, CdOimplanted hexagonal ZnO nanoplatelets: red-shifted emission and enhanced charge carrier-resistance and bacteria-inactivation, Appl. Phys. A 125, (2018) 14

[9] R. Uma, K. Ravichandran, S. Sriram, B. Sakthivel, Cost-effective fabrication of ZnO/g-C3N4 composite thin films for enhanced photocatalytic activity against three different dyes (MB, MG, and RhB), Mater. Chem. Phys. 201, (2017) 147–155

[10] S. Snega, K. Ravichandran, N.J. Begum, K. Thirumurugan, Enhancement in the electrical and antibacterial properties of sprayed ZnO films by simultaneous doping of Mg and F, J. Mater. Sci. Mater. Electron. 24, (2013) 135–141

[11] A. El Hichou, M. Addou, A. Bougrine, R. Dounia, J. Ebothé, M. Troyon, M. Amrani, Cathodoluminescence properties of undoped and Al-doped ZnO thin films deposited on glass substrate by spray pyrolysis, Mater. Chem. Phys. 83, (2004) 43–47

[12] C.G. Jin, T. Yu, Z.F. Wu, F. Wang, M.Z. Wu, Y.Y. Wang, Y.M. Yu, L.J. Zhuge, X.M. Wu, Room-temperature deposition of transparent conductive Al-doped ZnO thin films using low energy ion bombardment, Appl. Phys. A 106, (2012) 961–966

[13] M. Alexiadou, M. Kandyla, G. Mousdis, M. Kompitsas, Pulsed laser deposition of ZnO thin films decorated with Au and Pd nanoparticles with enhanced acetone sensing performance, Appl. Phys. A 123, (2017) 262

[14] H. Liang, Q. Feng, X. Xia, R. Li, H. Guo, K. Xu, P. Tao, Y. Chen, G. Du, Room temperature electroluminescence from arsenic doped p-type ZnO nanowires/n-ZnO thin film homojunction light-emitting diode, J. Mater. Sci. Mater. Electron. 25, (2014) 1955– 1958

[15] H.T. Cao, C. Sun, Z.L. Pei, A.Y. Wang, L.S. Wen, R.J. Hong, X. Jiang, Properties of transparent conducting ZnO: Al oxide thin films and their application for molecular organic light-emitting diodes, J. Mater. Sci. Mater. Electron. 15, (2004) 169–174

[16] S. Li, G. Fang, H. Huang, H. Long, H. Wang, X. Mo, B. Dong, X. Zhao, Tunability of UV electroluminescence for n-ZnO: Al/nZnO/i-MgO/n-GaN heterostructured light-emitting diodes, Appl. Phys. B 107, (2012) 497–502

[17] A.A. Rani, S. Ernest, Characterization of spray-deposited ZnO thin films for dye-sensitized solar cell application, Appl. Phys. A 122, (2016) 647

[18] R. Fan, F. Lu, K. Li, Single-mode channel waveguide at 1540nm in Er-doped ZnO thin film, J. Lumin. 192, (2017) 410–413

[19] S.L. Li, F.M. Deng, Y.K. Ye, G. Fu, B. Liu, F.X. Wang, H.L. Wang, Optical waveguide and 1.54 μm photoluminescence properties in RF sputtered Er/Yb-doped ZnO thin films, Thin Solid Films 596, (2015) 51–55

[20] S. Khodja, T. Touam, A. Chelouche, F. Boudjouan, D. Djouadi, Z. Hadjoub, A. Fischer, A. Boudrioua, Effects of stabilizer ratio on structural, morphological, optical and waveguide properties of ZnO nanostructured thin films by a sol–gel process, Superlattices Microstruct. 75, (2014) 485–495

[21] P. Gu, X. Zhu, D. Yang, Effect of annealing temperature on the performance of photoconductive ultraviolet detectors based on ZnO thin flms, Appl. Phys. A 125(2019), 50

[22] M. Mazhdi, M.J. Tafreshi, The effects of gadolinium doping on the structural, morphological, optical, and photoluminescence properties of zinc oxide nanoparticles prepared by co-precipitation method, Appl. Phys. A 124, (2018) 863

[23] J.-H. Shen, S.-W. Yeh, H.-L. Huang, D. Gan, N.-J. Ho, Lowtemperature preparation of undoped ZnO films with high transparency and conductivity by ion beam deposition, J. Electron. Mater. 39, (2010) 612–618

[24] P. Shukla, S. Tiwari, S.R. Joshi, V.R. Akshay, M. Vasundhara, S. Varma, J. Singh, A. Chanda, Investigation on structural, morphological and optical properties of Co-doped ZnO thin films, Phys. B 550, (2018) 303–310

[25] E. Asikuzun, O. Ozturk, L. Arda, C. Terzioglu, Preparation, growth and characterization of nonvacuum Cu-doped ZnO thin films, J. Mol. Struct. 1165, (2018) 1–7

[26] A. Chelouche, D. Djouadi, H. Merzouk, A. Aksas, Influence of Ag doping on structural and optical properties of ZnO thin films synthesized by the sol–gel technique, Appl. Phys. A 115, (2014) 613–616

[27] A. Jilani, M.S. Abdel-Wahab, H.Y. Zahran, I.S. Yahia, A.A. AlGhamdi, Linear and nonlinear optical investigations of nanoscale Si-doped ZnO thin films: spectroscopic approach, Appl. Phys. A 122, (2016) 862

[28] D.K. Kim, K.M. Kim, C.B. Park, Characteristics of p-type ZnO: As thin films prepared by the ampoule-tube method and ZnO p–n homojunction, Appl. Phys. A 98, (2010) 913–917

[29] Y. Kim, J. Choe, G. Nam, I. Kim, J.-Y. Leem, S.-H. Lee, S. Kim, D.Y. Kim, S.-O. Kim, Influence of Al-, Co-, Cu-, and In-doped ZnO buffer layers on the structural and the optical properties of ZnO thin films, J. Korean Phys. Soc. 66, (2015) 224–228

[30] A. Jamil, S. Fareed, N. Tiwari, C. Li, B. Cheng, X. Xu, M.A. Rafiq, Effect of titanium doping on conductivity, density of states and conduction mechanism in ZnO thin film, Appl. Phys. A 125, (2019) 238

[31] S.P. Bharath, K.V. Bangera, G.K. Shivakumar, Enhanced gas sensing properties of indium doped ZnO thin films, Superlattices Microstruct. 124, (2018) 72–78

[32] C.S. Prajapati, A. Kushwaha, P.P. Sahay, Optoelectronics and formaldehyde sensing properties of tin-doped ZnO thin films, Appl. Phys. A 113, (2013) 651–662

[33] T. Hojati, M. Ebrahimi, R. Afzalzadeh, Highly sensitive CO sensor based on ZnO/MWCNT nanosheet network grown via hydrothermal method, Mater. Chem. Phys. 207, (2018) 50–57

[34] A.S. Kumar, K.K. Nagaraja, H.S. Nagaraja, Effect of Sn doping on structural, optical, electrical and wettability properties of oriented ZnO nanorod arrays, J. Mater. Sci. Mater. Electron. 24, (2013) 3812–3822

[35] A. Nirmal, A.K.K. Kyaw, X. Sun, H.V. Demir, Demonstration of the portability of porous microstructure architecture to indium-doped ZnO electron selective layer for enhanced light scattering in inverted organic photovoltaics, J. Sol Gel Sci. Technol. 78, (2016) 613–620

[36] M. Taheri, H. Abdizadeh, M.R. Golobostanfard, Hierarchical ZnO nanoflowers and urchin-like shapes synthesized via sol-gel electrophoretic deposition with enhanced photocatalytic performance, Mater. Chem. Phys. 220, (2018) 118–127

[37] L. Xu, J. Miao, Y. Chen, J. Su, M. Yang, L. Zhang, L. Zhao, S. Ding, Characterization of Ag-doped ZnO thin film for its potential applications in optoelectronic devices, Optik 170, (2018) 484–491

[38] C.-F. Fu, L.-F. Han, C. Liu, Effects of sputtering power on structural, electrical and optical properties of Cr-doped ZnO thin films prepared by magnetron sputtering, J. Mater. Sci. Mater. Electron. 26, (2015) 493–497

[39] Ghosh M, Dilawar N, Bandyopadhyay A K and Raychaudhuri A K Phonon dynamics of Zn(Mg, Cd)O alloy nanostructures and their phase segregation J. Appl. Phys. 2009 106 084306

[40] Zheng Y, Chen C, Zhan Y, Lin X, Zheng Q, Wei K, Zhu J, and Zhu Y Luminescence and photocatalytic activity of ZnO nanocrystals: correlation between structure and property Inorg. Chem. (2007) 46 6675–82

[41] Ibram Ganesh∗, P.S. Chandra Sekhar, G. Padmanabham, G. Sundararajan, Influence of Li-doping on structural characteristics and photocatalytic activity

of ZnO nano-powder formed in a novel solution pyro-hydrolysis route, Applied Surface Science (2012) 259 524– 537.